UNIVERSITY OF CALIFORNIA,

IRVINE

# Quantifying the Structural Composition of Induced Pluripotent Stem Cell Derived Cardiomyocytes and Porcine Esophageal Tissue

THESIS

Submitted in partial satisfaction of the requirements for the degree of

MASTER OF SCIENCE

in Biomedical Engineering

by

Mira Asad

Thesis Committee:

Associate Professor Anna Grosberg, Chair

Associate Professor Joshua Mauney

Associate Professor Michelle Digman

2021

## TABLE OF CONTENTS

## LIST OF FIGURES

## ACKNOWLEDGEMENTS

I would like to acknowledge my research advisor and committee chair, Dr. Anya Grosberg, for all her guidance and assistance throughout both my graduate and undergraduate studies. I would also like to thank my committee members, Dr. Joshua Mauney and Dr. Michelle Digman, for their feedback and assistance with the thesis writing process.

I would also like to thank all members of the Cardiovascular Modeling laboratory for their help and support throughout the years. I would especially like to thank Jasmine Naik, Tessa Morris, Richard Tran, and Emil Lundqvist for their mentorship and feedback throughout my master's program.

Lastly, I would like to acknowledge my family and friends who have kept me motivated and energized throughout this process.

## ABSTRACT OF THESIS

Quantifying the Structural Composition of Induced Pluripotent Stem Cell Derived Cardiomyocytes and Porcine Esophageal Tissue

By

Mira Asad

Master of Science in Biomedical Engineering

University of California-Irvine, 2021

Associate Professor Anna Grosberg, Chair

The heart and esophagus are two of many organs in the body that rely on tissue organization to function properly. For both, in the disease states, cytoskeletal structure is often compromised, leading to major complications. To better understand both healthy and diseased states in the heart and esophagus, this thesis quantified the structural organization of various cytoskeletal components. For the heart, the effect of the LMNA gene mutation on nuclei, sarcomere, and actin organization was elucidated using induced pluripotent stem cell (iPSC) derived cardiomyocytes from both patients and controls. There was significance in sarcomere organization between control and patient cell lines, but no significance was found with the orientation in actin fibrils. Additionally, it was concluded that there is no significant difference in the means of the percentages of dysmorphic nuclei between patient and control lines. To study esophageal structure, tissue sections were harvested from a porcine model and were stained for slow skeletal myosin heavy chain (SMHC) as well as sarcomeric z-lines. When quantifying the organization of SMHCs and z-lines in tissue sections sliced perpendicular to the lumen, it was

determined that there is a significant difference between the esophageal regions. However, there was no significant difference between the z-line orientation in the two esophageal regions for the longitudinally sliced tissue. Overall, studies showed that important quantitative metrics can be evaluated to reveal how these organs function.

## INTRODUCTION

In biological tissues, the multi-scale architecture of cellular components is essential for proper organ function. For example, in the heart it has been shown that structural organization and cytoskeleton alignment are important for maximizing peak force generation. Specifically, the increase in sarcomere alignment corresponded to an increase in peak systolic stress [1]. Another example is in the esophagus where the orientation of smooth muscle fibers assists in the transport of the bolus when contraction occurs [2]. Determining how cellular and tissue architecture affect function in any part of the body requires specific experimental tools.

There are multiple tools to study tissue architecture; including tissues engineered in vitro as well as tissue sections taken from animal models. Engineered tissue *in vitro* requires cell culturing in either a 2D or 3D state. Commonly, 2D cell culture has been used for its simplicity and efficiency [3]. Cell culture can be performed with various cell types, including those harvested from animals, or stem cells that can be programmed into the cell type needed. A limitation with cell culture is the variability and heterogeneity of tissue architecture [4]. Obtaining tissue sections from organs is another tool to investigate structural composition. A benefit of using tissue slices is that their organizational integrity and normal structure are maintained, but they are only viable for a short period of time [5,6]. For either method, to visualize cellular components, brightfield and fluorescence microscopy are tools that can be used. Brightfield microscopy is one of the simplest imaging techniques and has recently shown to be useful in cell detection and automated image analysis of cell populations [7,8]. However, there is poor contrast since cells are nearly transparent when no specific staining is applied, and therefore subcellular phenomena cannot be detected [8]. As a result, fluorescence microscopy is the standard visualization tool for analysis of cell function as it allows for only the object of interest to be revealed in an otherwise black

background [8,9]. Traditional wide-field fluorescence microscopes have great resolution, contrast, sensitivity, and acquisition speeds. For thicker samples such as tissue, contrast is reduced due to the out-of-focus features which blur the image [10]. In this circumstance, confocal laser-scanning microscopes should be used to obtain optimal images. Once images of the biological constructs have been obtained, analysis needs to be performed to quantify their structural organization.

There are multiple ways of analyzing tissue constructs, including both qualitative and quantitative approaches. Methods such as histology and western blot are two prominent qualitative analysis tools [11,12]. Histology is the study of microscopic anatomy in biological tissue, and western blot analysis is a technique to detect the presence of specific proteins in a tissue sample. However, with all qualitative methods, there is always some level of inherent bias. Additionally, visual inspection of biological structure in images along with manual measurement is labor intensive and results are potentially inaccurate [13]. Utilizing quantitative image analysis techniques eliminates user bias and helps in reducing manual labor and increasing accuracy, objectivity, and reproducibility [13,14]. To get accurate results, these quantitative approaches need to be customized to the specific organ being evaluated.

In this master's thesis, we present multiple examples of this workflow. In chapter one, we discuss the organization of nuclei, actin, and sarcomeres in induced pluripotent stem cell derived cardiomyocytes from patients with a LMNA gene mutation and related controls. Methods utilized in this section include culturing the heart tissue layer, immunofluorescence staining for the structures of interest, imaging the cardiac tissue on a confocal microscope, and analyzing the cellular structures using customized codes. The second chapter explores the structure of cellular components, such as slow myosin heavy chains and z-lines, in porcine esophageal tissue. By quantitively examining these structures, we hope to further understand the microscopic

mechanisms behind esophageal function to improve treatment options. To do this, tissue sections from a porcine model were fixed, immunofluorescence stained, and mounted with a glass coverslip on a microscope slide. Images were obtained on both a wide-field fluorescence and confocal microscope, and then organizational order was quantified using custom codes. The methods presented here can be a pathway to quantifying biological architecture and furthering the understanding of how each part of the body properly functions.

# CHAPTER 1

## Quantifying Structural Organization in iPSC-derived Cardiomyocytes

### 1.1 Introduction

Cardiovascular diseases affect millions of individuals each year and is the leading cause of death in the U.S., encompassing a wide range of issues with the heart such as arrhythmias, valve failures and hardening of the arteries among others [15]. One such disease, dilated cardiomyopathy (DCM), affects the heart muscle, causing it to become stiffer, often leading to heart failure [16]. Genetic DCM, or familial dilated cardiomyopathy (FDC), is inherited within familial generations through autosomal dominant genes [17]. One such gene whose mutation causes cardiac complications is the LMNA gene. The LMNA gene codes for intermediate filament proteins, Lamin A and Lamin C. They form a mesh like layer under the nuclei envelope which stabilizes the structure and shape of the nuclei. Nuclear Lamina mutation causes structural defects such as blebbing in the nuclei [18]. To quantify these defects, as well as additional structural information such as sarcomere organization, cells containing the mutation must be evaluated *in vitro*. In this chapter, we utilize induce pluripotent stem cell (iPSC) derived cardiomyocytes from patients containing the LMNA mutation, as well as both related and unrelated controls, to quantify the differences in structural organization.

### 1.2 Methods and Materials

Substrate Creation

Coverslips were made for structural assessment of the iPSC-derived cardiomyocytes. A 7.6cm x 8.3cm rectangular glass coverslip (Fisher Scientific Company, Hanover Park, IL) was cleaned in 200 proof ethanol with 30 min of sonication. The cleaned glass coverslip was then spin-coated with a 10:1 mixture of polydimethylsiloxane [PDMS] and curing agent (Ellsworth Adhesives, Germantown, WI) and cured in a 60 °C oven for 12 hours. Following this, the large, coated glass coverslips were cut into 14mm x 12.5mm rectangular pieces using a diamond cutter (VWR, Radnor, PA) [19,20].

Extracellular Matrix Microcontact Printing

To make 20 μm x 5 μm line patterned stamps, PDMS with curing agent (1:10 ratio) was poured onto a petri dish containing the silicon wafer, which was prepared by photolithography techniques. It was cured overnight in 60$^{o}$C oven. The cured PDMS with the printed patterns was removed from the petri dish and cut into square stamps. PDMS stamps were sonicated with 95% ethanol and coated in 100 μg/mL fibronectin (Fisher Scientific Company, Hanover Park, IL) for 1 hour. PDMS coated glass coverslips were UVO-treated for 8 minutes prior to being stamped with fibronectin coated 20x5 line stamps. Coverslips were placed completely in 1% Pluronic acid solution (5g Pluronics F-127, Sigma Aldrich, Inc., Saint Louis MO, dissolved in 500 mL sterile water) for 5 minutes to prevent cell adhesion outside the line pattern and then washed three times with PBS (Life Technologies, Carlsbad, CA) and stored in PBS at 4$^{o}$C until use [19,20].

Cell Culture

Prior to obtaining skin biopsies from participants for this project, informed consent was acquired in accordance with the UC Irvine Institutional Review Board (IRB# 2014-1253). Cell

lines used for this work were secured from skin biopsies of four different female participants, two healthy controls (CA1 and CA3) and two patients (PA1 and PA3, both have a heterozygous LMNA splice-site mutation (c.357-2A>G)), as well as a female commercial line (D2, (Lonza (catalog# CC-2511)). Skin biopsies were collected as described by Zaragoza, et al. [17] Fibroblast lines were reprogrammed with CytoTune-iPS 2.0 Sendai reprogramming kit (ThermoFisher Scientific, Cat# A16517) into induced Pluripotent Stem Cells [iPSCs]. iPSCs were seeded and passaged on Geltrex (Gibco, Cat# A1413302) or Vitronectin (Gibco, Cat# A1470) coated plates and fed with complete E8 media (Gibco, Cat# A15170) daily for seven days or until confluency has reached 80-90%. Following this, iPSC colonies were passaged with ReLeSR (StemCell Technologies, Cat# 05872) to the 15$^{th}$ passage to eliminate the Sendai virus from cultures. iPSC colonies were then singularized with TrypLE (Gibco, Cat# 12604-013) and seeded on Vitronectin or Geltrex coated 12-well plates at the desired density that would maximize cardiomyocytes differentiation efficiency for each cell line. Singularized cells were differentiated with *PSC Cardiomyocyte Differentiation Kit* (Gibco, Cat#A2921201). Around the 9$^{th}$ day of differentiation beating clusters were observed and purification of the culture was performed using Enriched Cardiomyocytes Media (ECM, Gibco, Pub. # MAN0014509), to greatly reduce the number of non-cardiomyocytes. On the 16$^{th}$ day of differentiation, purified cultures were dissociated with STEMdiff™ Cardiomyocyte Dissociation Kit (StemCell Technologies, Cat# 05025). Cardiomyocytes were then seeded onto the patterned coverslips with supporting cardiomyocyte media from STEMdiff™ kit, and they were fed with M199 media with 10% FBS after 24 hours and with 2% FBS after 48 hours from seeding. After these four days, the cells are ready to be fixed and stained.

Fixing and Immunostaining

Cells were fixed for ten minutes at room temperature with a solution of of 4% Paraformaldehyde [PFA] (Fisher Scientific Company, Hanover Park, IL) and 0.05% Triton X-100 (Sigma-Aldrich, Saint Louis, MO). 4% PFA with 0.05% Triton X-100 was made by diluting 16% PFA with PBS and warming in a 37$^{o}$C water bath. Cells were washed three times with PBS and incubated in the PFA/Triton-X solution for ten minutes. Following incubation, cells were again washed three times with PBS (5-minute wait between each wash) and stored in PBS until immunostaining.

Primary antibodies including sarcomeric α-actinin (Mouse Monoclonal Anti-a-actinin, Sigma Aldrich, Inc., Saint Louis, MO), 4',6'-diaminodino-2- phenylindole (DAPI) (Life Technologies, Carlsbad, CA), Alexa Fluor 488 Phalloidin (Life Technologies, Carlsbad, CA) were used when staining for sarcomeres, nuclei, and actin, respectively. Secondary staining was done using the Alexa Fluor 630 goat anti-mouse antibody (Life Technologies, Cat# A121050). Coverslips were then mounted on to microscope slides with Prolong Gold Antifade Mount and sealed with clear nail polish. The slides are left to dry overnight and are then imaged [19, 20].

Imaging and Image Analysis

Samples were imaged using a Leica SP8 confocal microscope with 63x (5.54 μm/pixel) oil immersion objective. For each sample, ten fields of view were randomly selected and imaged. Analysis for structural information, such as the orientational order parameter, was conducted using customized MATLAB software provided by the Grosberg Lab [20, 21].

Statistics

For structural data, the student t-test was used to compare single pairs of data, and ANOVA with Student-Newman-Keuls post hoc test was used for multi-pair comparison. Significance was determined for p-value less than 0.5.

### 1.3 Results

The aim of this study was to evaluate the structural organization of nuclei, actin, and sarcomeres in iPSC-derived cardiomyocyte from patients with the LMNA gene mutation and healthy controls (both related and unrelated). To do this, my collaborators cultured and differentiated the iPSCs into cardiomyocytes *in vitro*. Following this, cells were seeded onto coverslips, fixed, and stained for the three previously mentioned structures. The slides were imaged on a confocal scope and custom MATLAB codes were used to quantify information such as nuclei dysmorphism, nuclei area, and the Orientational Order Parameter (OOP).

To evaluate the effects of the LMNA gene mutation on nuclei composition, each nucleus was extracted from the image stack using a custom code (example image of extraction in Figure 1.1 B). Following extraction, the nuclei were analyzed for dysmorphic percentage and area. There was no significant difference observed in the mean of the percentages of the dysmorphic nuclei between patients and controls (Figure 1.1C). However, there was a significant difference in the nuclei area between PA1 and controls as well as PA1 and PA3 (Figure 1.1C).

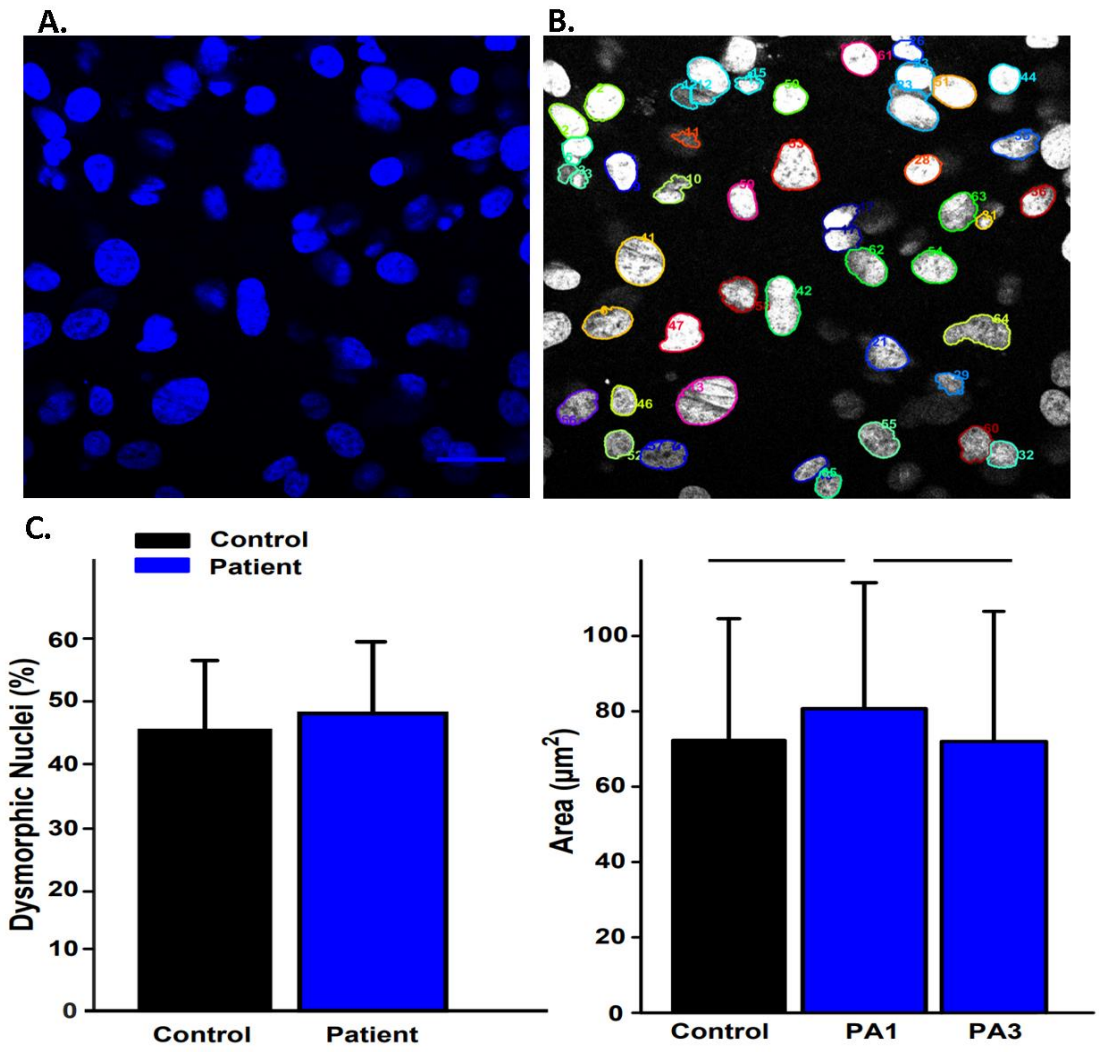


**Figure 1.1 Nuclei Classification of Patient and Control iPSC-derived Cardiomyocytes.** (A) Confocal image of nuclei (DAPI) from PA3. Scale bar: 25 μm. (B) Example image of nuclei identification from analysis code. (C) Plots of the mean of the percentages of dysmorphic nuclei (sample size based on number of coverslips; n=32 for control and n=27 for patient) and average area of nuclei in patients and controls (sample sized based on number of cells; n=3955 for control, n=3086 for PA1, and n=1510 for PA3). Error bars indicate standard deviation and black bars indicate significant difference ($p<0.05$).

Next, we looked at the organization of both sarcomeres and actin fibrils to determine if there was a significant difference between controls and patients. To evaluate this, the OOP was calculated for both structures utilizing custom codes. In Figure 1.2 A-H, there are representative images for patients and controls as well as example images of the code output. There was a

significant difference in sarcomere orientation between PA3 and all other control and patient lines (Figure 1.2 I). However, there was no significant difference observed in the OOP of actin among the cell lines.

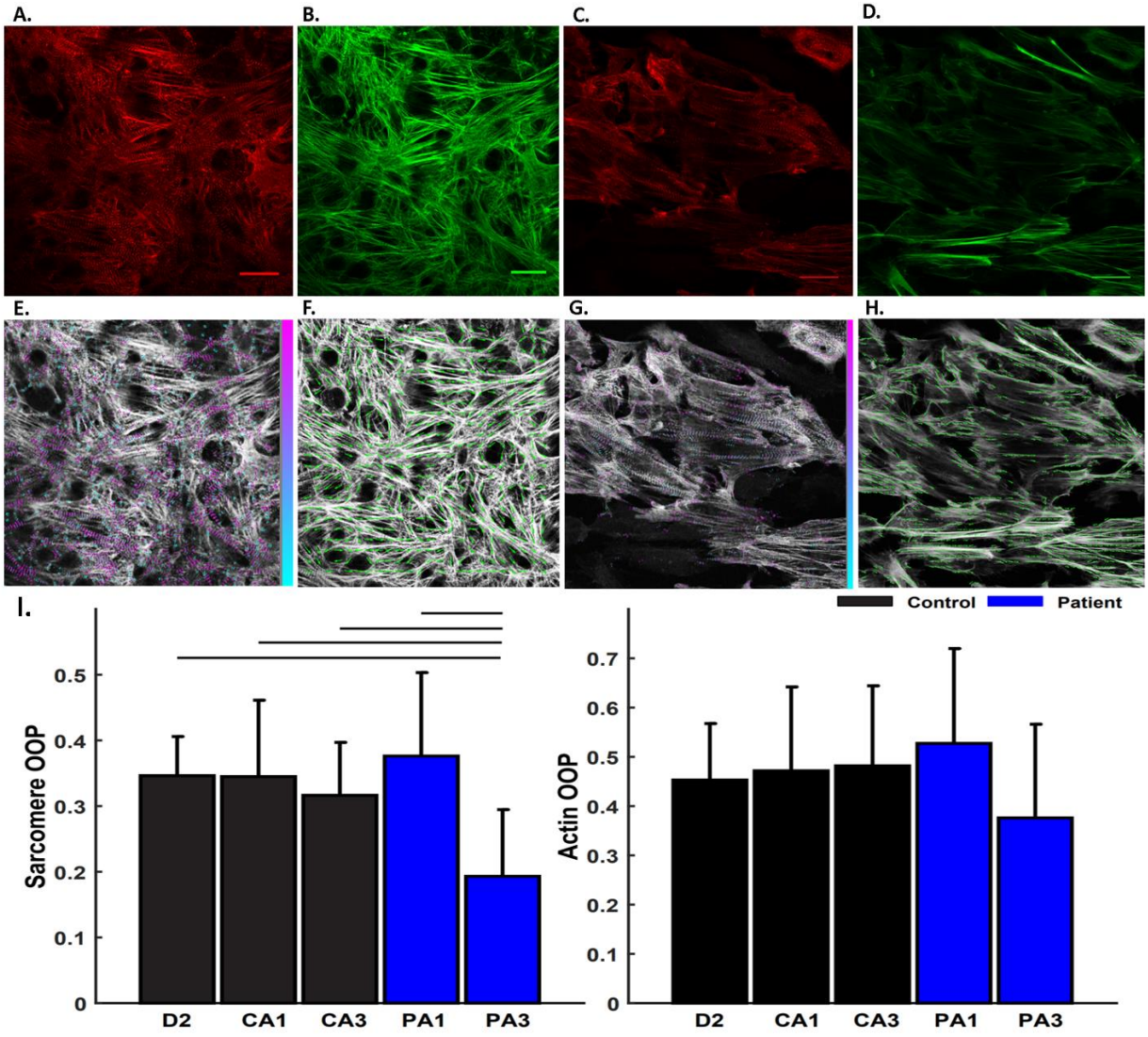


**Figure 1.2 Organization of Sarcomere and Actin in iPSC-derived Cardiomyocytes.** (A-D) Confocal images stained for sarcomeres (red) and actin fibrils (green). (E-H) Example analysis of actin orientation (green arrows) and sarcomere identification (purple and blue) for images A-D. (I) Average Orientational Order Parameter (OOP) of sarcomere and actin fibril in both patients and controls. Error bars indicate standard deviation and black bars indicate significant difference ($p<0.05$).

## 1.4 Discussion and Future Direction

In this work, iPSC-derived cardiomyocytes were used as an *in vitro* platform to evaluate the cellular organization of components such as nuclei, actin fibrils, and sarcomeres in patients with a LMNA mutation as well as healthy controls. We showed that large quantities of structural data can be processed and evaluated for various metrics such as dysmorphia percentage, area, and the OOP. When evaluating the nuclei, there was not a significant difference in the mean dysmorphic percentage, however there was a significant difference in area among the PA1 cell line compared to the controls and PA3 (Figure 1.1C). This may indicate that rather than evaluating the number of dysmorphic nuclei, it is the degree of dysmorphia which should be assessed. Quantifying the OOP of sarcomeres yielded significance between PA3 and all other cell lines. It is important that, overall, all OOP values were on the lower end (less than 0.5) but the PA3 line was significantly more isotropic. These low OOP values can be attributed to the general immaturity of iPSC-derived cardiomyocytes [22].

Moving forward, it would be interesting to compare how nuclei area relates to severity of dysmorphia. Additionally, utilizing animal models that contain the gene mutation, and ones that do not, may yield more significance in the organizational order parameter of sarcomeres since the maturation of cardiomyocytes would be greater.

# CHAPTER 2

## Quantifying Structural Organization in Porcine Esophagus Tissue

### 2.1 Introduction

Esophageal cancer is the 8$^{th}$ most common cancer in the world and has a poor prognosis, accounting for an estimated four hundred thousand deaths annually [23,24]. Esophageal repair or replacement via tissue engineered scaffolds is a common procedure to treat patients with squamous cell carcinoma and adenocarcinoma [24,25]. Throughout the years, a multitude of different materials such as rubber, polyethylene, Teflon, and others have been used for scaffold creation. In the long-term, most of these materials were eventually removed as leakages were common and stenosis often developed [26]. Additionally, newer approaches such as stimulating regeneration of native tissue, or creating tissue-engineered neoesophagus using cells, have had issues in replicating the composition and functionality of the original esophagus [26]. Further understanding of healthy esophageal components, including the external muscle layer, is needed for treatment enhancement.

Present in the outer-most layer of the esophagus is the muscularis externa, containing an inner circular layer and outer longitudinal layer [24,27,28]. Experiments have shown that muscle activation of these layers plays a key role in esophageal transport [29]. However, studies conducted concerning the coordination between the two muscle layers have yielded conflicting results likely due to investigators using different recording techniques [30]. Additionally, there is little known regarding the connection between the functional role of these layers and their structural composition, particularly the longitudinal layer [28]. Most findings focus on the macroscopic level, putting emphasis on the integrated function of these muscle layers during peristalsis [29, 30]. To treat disease states, it is important to fully understand the structural composition of the healthy

esophagus at the cellular and tissue level. Elucidating the cellular architecture leads to the improvement of scaffold creation and tissue regeneration for the esophagus. This chapter details preliminary results regarding structural organization of porcine esophageal tissue and future work that must be completed. This works was done in collaboration with Dr. Joshua Mauney's Lab at the UC Irvine Medical Center.

## 2.2 Methods and Materials

Fixation and Sectioning of Tissue

All esophagus tissue samples used in this work were harvested from healthy, control swine models. Following animal sacrifice, tubular esophageal regions were washed with PBS to remove any particles and blood. Regions no larger than 5 mm in thickness were fixed in 10% neutral-buffered formalin overnight and then placed in PBS or 70% ethanol (if the sample is being kept more than a day prior to paraffin embedding). Samples should be sent to paraffin embedding 6-24 hours after PBS hydration. Once embedded, tissues were sectioned into 5-micron slices and placed onto microscope slides, ready to for staining [31].

Deparaffinization and Immunofluorescence Staining

To begin the immunostaining process, the samples are deparaffinized with xylene and then rehydrated in ethanol. Primary antibodies including sarcomeric α-actinin (Mouse Monoclonal Anti-a-actinin, Sigma Aldrich, Inc., Saint Louis, MO), 4',6'-diaminodino-2- phenylindole (DAPI) (Life Technologies, Carlsbad, CA), anti-slow skeletal myosin skeletal heavy (MYH) (Abcam, Cambridge, MA, USA), anti-α-smooth muscle actin (SMA) (Sigma-Aldrich, St. Louis, MO, USA; 1:200 dilution) were used at a 1:200 dilution when staining for sarcomeres, nuclei, slow skeletal myosin, and smooth muscle actin respectively. Species-matched Alexa Fluor 488, 594 and 633

conjugated antibodies were used for secondary staining. Following, slides were mounted with Prolong Gold Antifade Mount (Life Technologies, Carlsbad, CA) and rectangular glass coverslips, sealed with clear nail polish, and dried overnight. For a complete step by step protocol, please refer to the appendix.

Imaging and Image Analysis

Tissue samples were imaged using both fluorescence and confocal microscopy. Fluorescent imaging was done using the IX-83 inverted motorized microscope (Olympus America, Center Valley, PA) mounted with a digital CCD camera ORCAR2 C10600-10B (Hamamatsu Photonics, Shizuoka Prefecture, Japan) and an UPLFN 40x oil immersion objective (Olympus America, Center Valley, PA). Confocal imaging was performed using the Olympus Fluoview FV3000 with 30x (8.351 μm/pixel) and 40x (μm/pixel) oil immersion objectives. For each sample, a variable number of images were taken to capture the present alpha actinin or slow myosin heavy chain. Analysis was done on the images using customized MATLAB software provided by the Grosberg Lab [21].

Statistics

One-way ANOVA with Tukey test were performed for pairwise comparison of esophageal regions. Significance was determined for p-value less than 0.05.

**2.3 Results**

The aim of this study was to quantify the structural organization of skeletal muscle in the esophagus. To do this, tissue sections, sliced perpendicular to the esophageal lumen axis, were obtained from a healthy swine model and stained for skeletal muscle markers. These sections were then imaged using both a fluorescence microscope and confocal microscope to analyze the

composition of the circular and longitudinal muscle layers. To evaluate the organization of the slow skeletal myosin heavy chains (SMHC) and z-lines in the images, a custom MATLAB code was used to quantify the Orientational Order Parameter (OOP) which obtains the degree of order of each structure in each esophageal region; cervical, thoracic, and abdominal (see Figure 2.1 D for cartoon schematic of esophageal layers). For each image, the code generated on OOP value between 0 and 1. An OOP value close to 0 indicates the structure is isotropic (not aligned) and a value close to 1 means the structure is anisotropic (highly aligned).

The first round of tissue sections was stained using anti-slow skeletal myosin since it is a common marker of skeletal maturation in the esophagus [31]. As seen in Figure 2.1 A-C, all three regions of the esophagus were positive for this marker. In the cervical region, the SMHCs appear to be more fragmented in comparison to the sections from the thoracic and abdominal region. Additionally, the cervical section has more background present that is not positive for SMHC in comparison to the other two sections. This is contributing to the lower OOP values overall since the OOP was quantified without eliminating structures that are not SMHCs. There is a significant difference between the cervical and thoracic region, as well as between the cervical and abdominal regions. Between the thoracic and abdominal regions, no significant difference in the OOP was observed. Overall, all three regions had a lower OOP (under 0.5) due to the excess background picked up in the images.

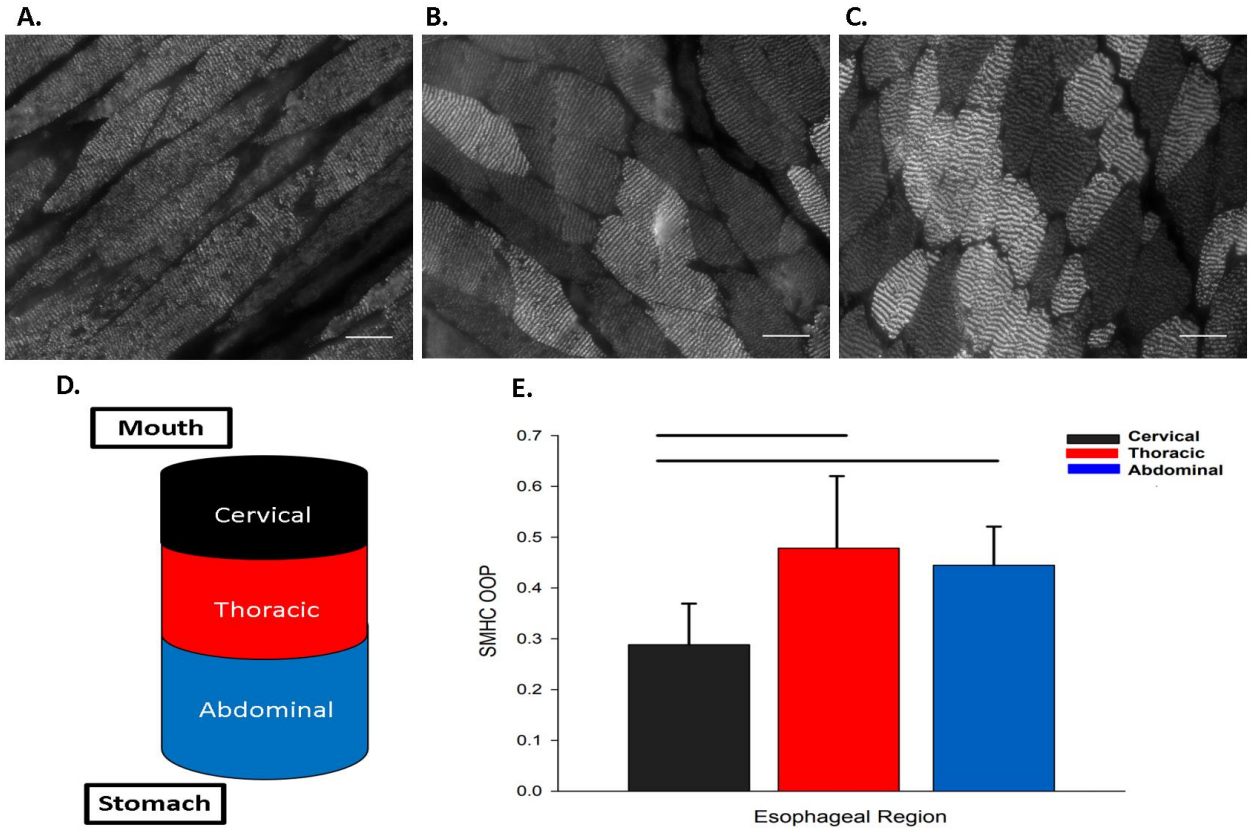


**Figure 2.1 Organization of Slow Skeletal Myosin Heavy Chains (SMHC) in Porcine Esophageal Tissue.** (A-C) Immunofluorescence-stained images of slow myosin heavy chain (red) in the cervical (A), thoracic (B), and abdominal (C) region of the esophagus. Scale bar: 25 μm. (D) Cartoon representation of the esophageal layer locations. (E) Average Organizational Order Parameter of SMHC in the three esophageal layers (sample size based on fields of view; n=20 for cervical, n=15 for thoracic, and n=20 for abdominal). Note: all samples came from a single porcine model. Error bars indicate standard deviation and black bars indicate significant difference ($p<0.05$).

Following the staining of SMHC, we looked at the organization of sarcomeres in the longitudinal and circular layer of the esophagus, since it is the functional unit of contraction. Though SMHC was present in all regions, the abdominal region of the esophagus was not positive for the alpha-actinin stain. Images of the cervical and thoracic region (Figure 2.2 A-B) were obtained since both contained the z-line architecture. When quantifying the preliminary data, there is a significant difference in the average OOP between the two regions (Figure 2.2 C). Although there is still background interference in this case, this significant difference points to the functional

roles of these regions. In the cervical region, there is the greatest amount of skeletal muscle, and it is where muscle contraction is initiated during peristalsis [30]. Therefore, the higher OOP value points to the needed alignment of z-lines to have proper esophageal function.

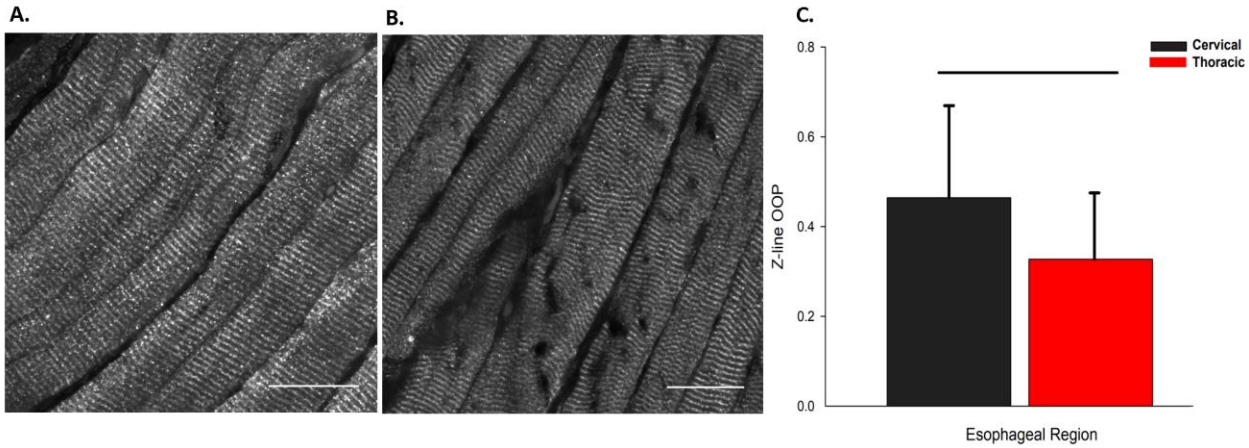


**Figure 2.2 Organization of Z-lines in Porcine Esophageal Tissue.** (A-B) Immunofluorescence-stained images of sarcomeric z-lines in the cervical (A) and thoracic (B) regions. Scale bar: 25 μm. (C) Average Orientational Order Parameter of Z-lines in each esophageal layer (sample size based on fields of view; n=35 for cervical and n=26 for thoracic). Note: all samples came from a single porcine model. Error bars indicate standard deviation and black bars indicate significant difference ($p<0.05$).

Lastly, we evaluated the organization of z-line architecture in the esophagus when it was sliced in parallel with the lumen. Such a projection provides a view of the microscopic structure in the direction that it functions. As with the previous z-line staining, these longitudinally sliced pieces were also only positive for alpha-actinin in the cervical and thoracic regions (Figure 2.3 A-B). In this case, there was no significant difference between the average OOP values. However, in this case the average OOP values were higher in comparison to the perpendicularly sliced cases.

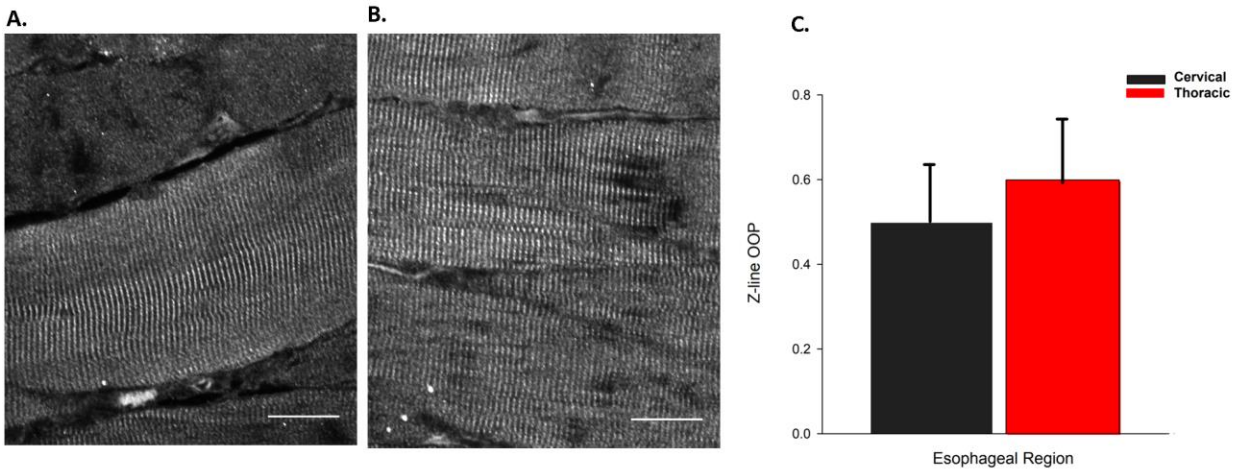


**Figure 2.3 Organization of Z-lines in Longitudinally Sliced Porcine Esophageal Tissue.** (A-B) Immunofluorescence-stained images of sarcomeric z-lines in the cervical (A) and thoracic (B) regions. Scale bar: 25 μm. (C) Average Orientational Order Parameter of Z-lines in each longitudinally sliced esophageal layer (sample size based on fields of view; n=8 for cervical and n=7 for thoracic). Note: all samples came from a single porcine model. Error bars indicate standard deviation and black bars indicate significant difference ($p<0.05$).

## 2.4 Discussion and Future Direction

In this preliminary study, we demonstrated the ability to quantify microscopic skeletal structures in a porcine esophagus model. In the first two cases with the SMHC and z-lines, significant differences were noted between the OOP. All regions had a relatively low OOP value due to background elements present in the evaluation of these specific markers. Additionally, the preliminary results of the longitudinally sliced tissue indicate they are aligned more than the perpendicularly sliced tissue sections. Functionally, the esophageal layers contract with coordination in the longitudinal direction and circular direction [29]. Therefore, it makes sense that the longitudinally sliced tissue sections of the longitudinal muscle are more organized than the slice of the longitudinal muscle in the direction perpendicular to the lumen.

In future work, it will be important to stain for F-actin and eliminate structures that are not SMHCs or z-lines from the image quantification in order to obtain more accurate information

about structure alignment. Also, looking at the organization of SMHC in longitudinally sliced tissue and comparing it to the perpendicular slices would be interesting. Additionally, it would be important to compare organizational data between multiple porcine models to determine the similarity and uniformity of structural organization from one pig to another. It would also be interesting to quantify the structure of diseased esophageal tissue and see how that information can be used to improve upon disease treatment options. In the long term, it would be of interest to implement this work in multiple animal models and look at the co-orientational order parameter [32] between structures such actin and sarcomere in each animal and compare them. Understanding which structural organization is important to function and which is not will help in creating better scaffolds for disease treatment.

## REFERENCES


[1] Feinberg AW, Alford PW, Jin H, Ripplinger CM, Werdich AA, Sheehy SP, Grosberg A, and K. K. Parker, "Controlling the contractile strength of engineered cardiac muscle by hierarchal tissue architecture," Biomaterials, vol. 33, pp. 5732-41, Aug 2012.

[2] Tan JY, Chua CK, Leong KF, Chian KS, Leong WS, Tan LP. "Esophageal tissue engineering: an in-depth review on scaffold design". Biotechnol Bioeng. 2012 Jan;109(1):1-15. Epub 2011 Sep 21.

[3] K. Duval, H. Grover, L. H, Han, Y. Mou, A. F. Pegoraro, J. Fredberg, Z. Chen. Modeling Physiological Events in 2D vs. 3D Cell Culture. Physiology (Bethesda). 2017 Jul;32(4):266-277.

[4] Arango MT, Quintero-Ronderos P, Castiblanco J, et al. "Cell culture and cell analysis". In: Anaya JM, Shoenfeld Y, Rojas-Villarraga A, et al., editors. Autoimmunity: From Bench to Bedside [Internet]. Bogota (Colombia): El Rosario University Press; 2013 Jul 18. Chapter 45.

[5] Haschek WM, Rousseaux CG, Wallig MA. "Chapter 6-Respiratory System". Fundamentals of Toxicologic Pathology (Second Edition). Academic Press. 2010. Pages 93-133.

[6] R.S. Settivari, J.C. Rowlands, D.M. Wilson, S.M. Arnold, P.J. Spencer. "Chapter 32 - Application of Evolving Computational and Biological Platforms for Chemical Safety Assessment". A Comprehensive Guide to Toxicology in Nonclinical Drug Development (Second Edition). Academic Press. 2017. Pages 843-873.

[7] G. Wang, N. Fang. "Chapter four - Detecting and Tracking Nonfluorescent Nanoparticle Probes in Live Cells". Methods in Enzymology. Academic Press. Volume 504. 2012. Pages 83-108.

[8] J. Selinummi, P. Ruusuvuori, I. Podolsky, A. Ozinsky, E. Gold, O.Yli-Harja, A. Aderem, I. Shmulevic. "Bright Field Microscopy as an Alternative to Whole Cell Fluorescence in Automated Analysis of Macrophage Images". PLoS One. Vol. 4, no. 10. 2009.

[9] Lichtman, J., Conchello, JA. "Fluorescence microscopy". Nat Methods 2, 910–919 (2005).

[10] Jonkman J., Brown C. "Any Way You Slice It—A Comparison of Confocal Microscopy Techniques'. J. Biomol Tech. 2015 Jul; 26(2): 54-56.

[11] Cohen MC, Aretz TH. "Histological Analysis of Coronary Artery Lesions in Fatal Postoperative Myocardial Infarction". Cardiovascular Pathology. Volume 8, Issue 3. 1999. Pages 133-139.

[12] MacPhee DJ, "Methodological considerations for improving Western blot analysis". Journal of Pharmacological and Toxicological Methods. Volume 61, Issue 2. 2010. Pages 171-177.

[13] Meijering E., Cappellen G.. (2007) "Quantitative Biological Image Analysis". In: Shorte S.L., Frischknecht F. (eds) Imaging Cellular and Molecular Biological Functions. Principles and Practice. Springer, Berlin, Heidelberg.

[14] Caicedo, J., Cooper, S., Heigwer, F. et al. “Data-analysis strategies for image-based cell profiling”. Nat Methods 14, 849–863 (2017).

[15] Nabel EG. “Cardiovascular Disease”. N Engl J Med 2003; 349:60-72.

[16] “Cardiomyopathy”. National Heart, Lung, and Blood Institute. Web.

[17] Zaragoza, M, Fung, L, Jensen, E, et al. “Exome Sequencing Identifies a Novel LMNA Splice-Site Mutation and Multigenic Heterozygosity of Potential Modifiers in a Family with Sick Sinus Syndrome, Dilated Cardiomyopathy, and Sudden Cardiac Death”. PLoS ONE 11.5 (2016).

[18] Lu, J. T., A. Muchir, P. L. Nagy, and H. J. Worman. “LMNA Cardiomyopathy: Cell Biology and Genetics Meet Clinical Medicine”. Disease Models & Mechanisms 4.5 (2011): 562-68. National Center for Biotechnology Information.

[19] Knight MB, Drew NK, McCarthy LA, Grosberg A. “Emergent Global Contractile Force in Cardiac Tissues”. Biophysical Journal. Volume 110, Issue 7. 2016. Pages 1615-1624.

[20] Core JQ, Mehrabi M, Robinson ZR, Ochs AR, McCarthy LA, Zaragoza MV, et al. (2017) “Age of heart disease presentation and dysmorphic nuclei in patients with LMNA mutations”. PLoS ONE 12(11).

[21] Morris TA, Naik J, Fibben KS, Kong X, Kiyono T, Yokomori K, et al. (2020) “Striated myocyte structural integrity: Automated analysis of sarcomeric z-discs”. PLoS Comput Biol 16(3).

[22] Giacomelli E, Meraviglia V, et. al. “Human-iPSC-Derived Cardiac Stromal Cells Enhance Maturation in 3D Cardiac Microtissues and Reveal Non-cardiomyocyte Contributions to Heart Disease”. Cell Stem Cell. 2020 Jun 4;26(6):862-879.

[23] Enzinger P, Mayer R. “Esophageal Cancer”. N Engl J Med 2003; 349:2241-2252.

[24] Tan JY, Chua CK, Leong KF, Chian KS, Leong WS, Tan LP. “Esophageal tissue engineering: an in-depth review on scaffold design”. Biotechnol Bioeng. 2012 Jan;109(1):1-15.

[25] Arakelian L, Kanai N, Dua K, Durand M, Cattan P, Ohki T. “Esophageal tissue engineering: from bench to bedside”. Ann N Y Acad Sci. 2018 Dec;1434(1):156-163.

[26] Fuchs JR, Nasseri BA, Vacanti JP. “Tissue engineering: a 21st century solution to surgical reconstruction”. Ann Thorac Surg. 2001 Aug;72(2):577-91.

[27] Yoshida M. “A light microscope study of the distribution of muscle in the frog esophagus and stomach”. J Smooth Muscle Res. 2001 Aug;37(3-4):95-104.

[28] Mittal RK. “Longitudinal muscle of the esophagus: its role in esophageal health and disease”. Curr Opin Gastroenterol. 2013 Jul;29(4):421-30.

[29] Kou W, Pandolfino JE, Kahrilas PJ, Patankar NA. “Simulation studies of circular muscle contraction, longitudinal muscle shortening, and their coordination in esophageal transport”. Am J Physiol Gastrointest Liver Physiol. 2015;309(4).

[30] Mittal RK. Regulation and dysregulation of esophageal peristalsis by the integrated function of circular and longitudinal muscle layers in health and disease. Am J Physiol Gastrointest Liver Physiol. 2016;311(3):G431-G443.

[31] Algarrahi K, Franck D, Cristofaro V, Yang X, Savarino A, Affas S, Schäfer FM, Ghezzi C, Jennings R, Nedder A, Kaplan DL, Sullivan MP, Estrada CR Jr, Mauney JR. “Bi-layer silk fibroin grafts support functional tissue regeneration in a porcine model of onlay esophagoplasty”. J Tissue Eng Regen Med. 2018 Feb;12(2):e894-e904.

[32] Drew NK, Eagleson MA, Baldo Jr. DB, Parker KK, Grosberg A (2015) “Metrics for Assessing Cytoskeletal Orientational Correlations and Consistency”. PLoS Comput Biol 11(4).

# Appendix:
# Immunofluorescence Staining Protocol for Paraffin Embedded Tissue Sections

Version 1.0

Protocol adapted from Dr. Joshua Mauney's lab at the UCI Medical Center

**Materials:**

- Slides containing tissue samples.
- Xylene
- Ethanol: 100%, 95%, 75%, 50% [in dH2O]
- 1X PBS
- 10 mM Sodium Citrate Buffer, pH 6 (2.94 g Sodium Citrate in 1L dH2O -> pH to 6 with HCL)
    - Dilute 20 mL of citrate buffer (10X) in 180 mL dH2O
- Blocking Buffer*
- Incubation Buffer*
- Primary and Secondary Antibodies
- ImmunoPen
- Coverslips

**Preparing Blocking Buffer (50 mL):**

Materials needed (can be made on lab benchtop):

- 50 mL conical
- 2.5 mL FBS
- 0.5 g BSA
- 150 ul TritonX
- 47.5 mL PBS

Add all these reagents into the 50 mL conical starting with the PBS. After PBS is in the conical, add FBS, BSA, and TritonX. Use a vortex to thoroughly combine all materials.

**Preparing Blocking Buffer (50 mL):**

Materials needed (can be made on lab benchtop):

- 50 mL conical
- 500 ul FBS
- 0.5 g BSA
- 49.5 mL PBS

Add all these reagents into the 50 mL conical starting with the PBS. After PBS is in the conical, add FBS and BSA. Use a vortex to thoroughly combine all materials.

**Day 1 Procedure:**

1. Begin by labeling slides with desired information using pencil.
2. Once labeled, heat slides at 55° C at 30 minutes to start the deparaffinization process.
3. Once the paraffin wax has melted, place the slides onto a rack and submerge in the first Xylene container for 5 min, then the second Xylene container for 5 min, and finally the third Xylene container for 5 MIN.

4. Rehydrate tissue in various reagents:
    1. 100% EtOH for 10 min, first container
    2. 100% EtOH for 10 min, second container
    3. 95% EtOH for 10 min, first container
    4. 95% EtOH for 10 min, second container
    5. 50% EtOH for 5 min
    6. $DH_2O$ for 5 min
    7. PBS for 5 min
5. Antigen Retrieval:
    1. Fill the container with sodium citrate buffer solution and warm it up for 30 seconds in the microwave.
    2. Place the slide rack in the container and begin the heating process. Slides will need to stay a total of ten minutes at 91-95 °C.
    3. Make sure to avoid boiling as slides are being microwaved (bubbles will dislodge tissue sections from slides).. If boiling occurs, stop the microwave until the liquid cools.
    4. This whole process will take longer than 10 min, but the total time of incubation in the 91-95 °C buffer needs to be 10 min. Use a thermometer to keep track of the temperature as well as a timer to ensure ten minutes of incubation time at the needed temperature.
    5. Allow for the slides to sit for 30 min at room temperature after the 10 minute incubation is complete.
6. Following this, use an ImmunoPen to circle each tissue section, Add blocking buffer to each section using a pipette. Leave the sections to incubate for 1 hr at room temperature.
7. Prepare primary antibodies up to the desired dilution in the blocking buffer( ie 1:200 would be 1 uL antibody for every 200 uL blocking buffer). Make sure to make enough antibody solution to cover all circled sections (each section should use 100-200 ul, depending on size).
8. Aspirate blocking buffer off slides, and add appropriate amount of primary antibody solution. Incubate overnight at 4 °C (in fridge or cold room).

**Day 2 Procedure:**

1. Wash off the primary antibody solution with PBS three times. Have PBS sit for 10 minutes between each wash.
2. Prepare the secondary antibody solution up to desired dilution in the incubation buffer.
3. After 3rd PBS wash, Pipette incubation buffer onto each tissue section. Incubate at room temp for one hour.
4. Wash off the secondary antibody solution with PBS three times. Have PBS sit for 10 minutes between each wash.
5. Mount slides with Prolong Gold antifade reagent and rectangular coverslips. Seal the coverslips with nail polish and let dry.
6. Store slides in -20 C if they are not being imaged immediately after staining.